Ca^{2+}-dependent Inactivation of Cardiac L-type Ca^{2+} Channels Does Not Affect Their Voltage Sensor

ROMAN SHIROKOV, RICHARD LEVIS, NATALIA SHIROKOVA and EDUARDO RÍOS

From the Department of Physiology, Rush University, Chicago, Illinois, 60612

ABSTRACT   Inactivation of currents carried by Ba^{2+} and Ca^{2+}, as well as intramembrane charge movement from L-type Ca^{2+} channels were studied in guinea pig ventricular myocytes using the whole-cell patch clamp technique. Prolonged (2 s) conditioning depolarization caused substantial reduction of charge movement between −70 and 10 mV (charge 1, or charge from noninactivated channels). In parallel, the charge mobile between −70 and −150 mV (charge 2, or charge from inactivated channels) was increased. The availability of charge 2 depended on the conditioning pulse voltage as the sum of two Boltzmann components. One component had a central voltage of −75 mV and a magnitude of 1.7 nC/μF. It presumably is the charge movement (charge 2) from Na$^+$ channels. The other component, with a central voltage of ~ −30 mV and a magnitude of 3.5 nC/μF, is the charge 2 of L-type Ca^{2+} channels. The sum of charge 1 and charge 2 was conserved after different conditioning pulses. The difference between the voltage dependence of the activation of L-type Ca^{2+} channels (half-activation voltage, $\overline{V}$, of ~ −20 mV) and that of charge 2 ($\overline{V}$ of −100 mV) made it possible to record the ionic currents through Ca^{2+} channels and charge 2 in the same solution. In an external solution with Ba^{2+} as sole metal the maximum available charge 2 of L-type Ca^{2+} channels was 10–15% greater than that in a Ca^{2+}-containing solution. External Cd^{2+} caused 20–30% reduction of charge 2 both from Na$^+$ and L-type Ca^{2+} channels. Voltage- and Ca^{2+}-dependent inactivation phenomena were compared with a double pulse protocol in cells perfused with an internal solution of low calcium buffering capacity. As the conditioning pulse voltage increased, inactivation monitored with the second pulse went through a minimum at about 0 mV, the voltage at which conditioning current had its maximum. Charge 2, recorded in parallel, did not show any increase associated with calcium entry. Two alternative interpretations of these observations are: (a) that Ca^{2+}-dependent inactivation does not alter the voltage sensor, and (b) that inactivation affects the voltage sensor, but only in the small fraction of channels that open, and the effect goes undetected. A model of channel gating that assumes

Address correspondence to Dr. R. Shirokov at Department of Physiology, Rush University, 1750 West Harrison Street, Chicago, Illinois, 60612.

Drs. Shirokov and Shirokova are on leave from the A.A. Bogomoletz Institute of Physiology, Ukrainian Academy of Sciences, Bogomoletz St. 4, 252601 GSP, Kiev 24, Ukraine.

the first possibility is shown to account fully for the experimental results. Thus, extracellular divalent cations modulate voltage-dependent inactivation of the Ca^{2+} channel. Intracellular Ca^{2+} instead, appears to cause inactivation of the channel without affecting its voltage sensor.

INTRODUCTION

Since the first recording of Ca^{2+} inward currents in cardiac tissue (Reuter, 1967) it became obvious that the slow rate of inactivation of this current is a key reason for the long plateau on the action potential. It was later shown that cardiac L-type Ca^{2+} channels possess both voltage and current-dependent inactivation (Kohlhardt, Krause, Kubler, and Herdey, 1975), which are similar to those of many other Ca^{2+} channels. Molecular mechanisms of these processes are yet to be understood (reviewed by Eckert and Chad, 1984). The measurement of charge movement allows one to detect molecular events when the channel is closed and it has been used as a tool in the analysis of inactivation of axonal Na^+ (reviewed by Armstrong, 1981), the voltage sensor of excitation-contraction coupling (VSECC, Brum and Ríos, 1987) and K^+ channels in expression systems (Bezanilla, Perozo, Papazian, Stefani, 1991; Stühmer, Conti, Stocker, Pongs, and Heinemann, 1991).

Fast voltage-dependent inactivation of Na^+ and K^+ channels was found to be accompanied by charge immobilization (Armstrong and Bezanilla, 1977; Bezanilla et al., 1991). Slow inactivation of Na^+ channels (Bezanilla, Taylor, and Fernandez, 1982), inactivation of the voltage sensor of excitation-contraction coupling of skeletal muscle (VSECC) and of cardiac Ca^{2+} channels (Brum and Ríos, 1987; Shirokov, Levis, Shirokova, and Ríos, 1992) were instead found to be accompanied by a shift of voltage dependence of their associated charge movements to negative voltages by ~80 mV.

We took advantage of this separation of the voltage distributions and designed a protocol to measure both ionic current through Ca channels (I_{Ca}) and charge movement (charge 2) currents in the same solutions, without using ionic current blockers. This technique allowed us to separate the contributions of two mechanisms to the inactivation of I_{Ca} and evaluate their effects on the voltage sensor. Some aspects of these results have been published in abstract form (Shirokov, Levis, Shirokova, and Ríos, 1993; Shirokov, Levis, and Ríos, 1993).

METHODS

Whole-cell currents were measured in single ventricular myocytes, enzymatically isolated from guinea pig hearts. Preparation of cells and current measurement were performed as described before (Shirokov et al., 1992). Briefly, cells were isolated from the ventricles of guinea pig hearts (strain Duncan-Hartley, 250–400 g) using 1.5 mg/ml collagenase (type I; Worthington Biochemical Corp., Freehold, NJ) and 0.3 mg/ml protease (type XXIV; Sigma Chemical Co., St. Louis, MO) applied by Langendorff perfusion. All experiments were carried out at at 19–22°C within 24 h after separation.

The composition of internal and external solutions is presented in Table I. The total concentration of external divalent cations was kept at 5 mM in all cases. All external solutions contained 0.5 mM Ba^{2+} which helped block residual outward currents and stabilized the baseline current. In the solution containing 4.5 mM Cd^{2+} and 0.5 mM Ba^{2+} no substantial ionic

currents were recorded at voltages from -150 to $+40$ mV. At variance with previous experiments, we used a Cs^+-based internal solution because intracellular TEA^+ affects cardiac calcium currents (Field, Hill, and Lamb, 1988). This seems a reasonable choice, as I_{Ca} was found to be identical in Cs^+- and K^+-containing solutions in pathological adult human ventricular cells having very small overlapping transient or background outward currents (Benitah, Bailly, Da Ponte, Delgado, and Lorente, 1992).

Voltage clamping (in the whole-cell mode of the patch clamp technique), pulse generation, and data acquisition were done with a commercial patch voltage clamp and associated hardware (Axopatch 1 series patch clamp with Axolab interface, under PC control, running PCLAMP software; Axon Instruments, Inc., Foster City, CA). The whole-cell capacitance circuitry of the Axopatch 1 was modified to allow compensation of most of the linear capacity transients, up to 300 pF. Additionally, the CLAMPEX program of PCLAMP was modified to allow data acquisition during conditioning pulses.

TABLE I

Ionic Composition of Internal and External Solutions

	External			Internal	
	Calcium	Barium	Cadmium	BAPTA	EGTA
Ca^{2+}	4.5	—	—	—	—
Ba^{2+}	0.5	5.0	0.5	—	—
Cd^{2+}	—	—	4.5	—	—
Cs^+	—	—	—	120	110
Mg ATP	—	—	—	5	5
TEA^+	166	166	166	—	—
HEPES	10	10	10	—	—
$EGTA^{2-}$	—	—	—	—	0.5
$BAPTA^{2-}$	—	—	—	10	—
Glucose	—	—	—	10	10
Creatine phosphate^{2-}	—	—	—	20	20
$Tris^+$	—	—	—	40	40
Aspartate$^-$	—	—	—	80	90
Cl^-	186	186	186	20	20
pH	7.25	7.25	7.25	7.80	7.80

Values are in mM. Osmolality, 310 mosmol/Kg.
TEA^+, Tetraethylammonium.
$EGTA^{2-}$, Ethylene glycol-bis(β-Aminoethyl ether) N, N, N', N'-Tetraacetic acid.
$BAPTA^{2-}$, 1,2-bis(2-Aminophenoxy)ethane N, N, N', N'-Tetraacetic acid.

Currents were filtered at 1 kHz (-3 dB, 4-pole Bessel filter) and sampled at 50–100 μs/point for charge movement measurements, or with slower rates for ionic current measurements.

A discussion of the quality of voltage clamp control and the effect of compensation of series resistance on the charge movement was presented before (Shirokov et al., 1992). Typical resistance of the pipettes was 1–2 $M\Omega$ when filled with internal solutions (Table I). After establishing the whole-cell configuration, the access resistance usually was 3–8 $M\Omega$ and routinely was compensated 70–90%. The holding potential (h.p.) was -90 mV. Asymmetric currents were obtained by subtraction of control currents elicited with pulses that took the membrane potential from -130 to -100 mV. The controls always preceded the test pulses (and conditioning pulses if applied). Sets of control and test pulses were applied at time intervals of 10–20 s. These precautions were taken to avoid the appearance of charge 2 in control pulses, that occurs with higher duty cycles. There was no sloping baseline correction.

RESULTS

Total Charge Is Conserved During Inactivation

It has been shown (Bean and Ríos, 1989; Hadley and Lederer, 1989; Shirokov et al., 1992), that the amount of charge associated with the opening of channels (mostly L-type Ca^{2+} and Na^+ channels) depends on the holding potential as a sum of two Boltzmann terms. On the other hand, due to inactivation, the voltage distribution of charge movement shifts toward negative voltages, causing reduction of the charge measured during test pulses to voltages that activate the channel (Shirokov et al., 1992). In the present work we followed the reduction of charge 1 and the appearance of charge 2 as a function of conditioning depolarization.
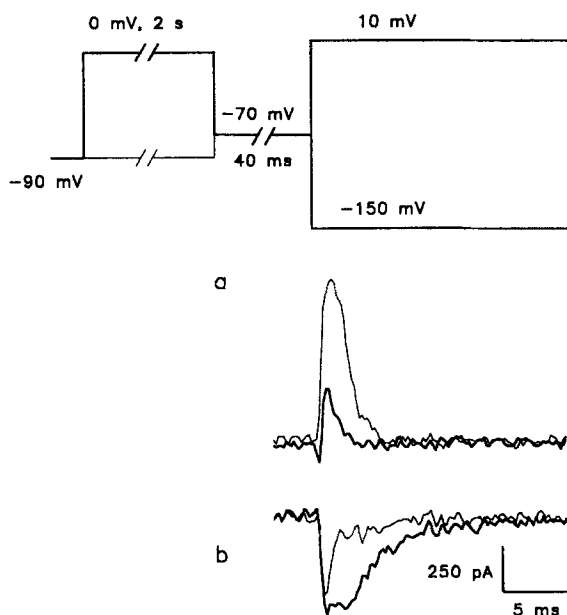

FIGURE 1. Effect of conditioning depolarization on charge movement elicited by a 25-ms pulse from −70 to 10 mV (current traces *a*), and from −70 to −150 mV (traces *b*). Asymmetric currents were obtained by pulses which were (*thick lines*) or were not (*thin lines*) preceded by conditioning to 0 mV for 2 s. Cell R1N19C51. $C_M = 156$ pF, $R_S = 5.4$ MΩ.

The effect of conditioning depolarization on availability of charge movement was studied as in previous works (e.g., Shirokov et al., 1992). One such study is illustrated in Fig. 1. The choice of the voltage in the interval during conditioning and test depolarizations (−70 mV) was based on our previous observation that, as in skeletal muscle, the distributions of charge 1 and charge 2 are separated by ~80 mV, and that −70 mV is a "watershed" voltage for these two classes of charge movement. First, a test pulse was applied (from −70) to +10 mV to monitor charge 1 available after conditioning. To block the ionic currents the experiment was performed in Cadmium external solution. Conditioning depolarization to 0 mV reduced the charge mobile between −70 and +10 mV (Fig. 1, current traces *a*). After that, the same protocol was repeated but the test pulse went from −70 to −150 mV. The same conditioning depolarization increased the charge mobile between−70 and −150 mV (Fig. 1,

current traces *b*). By varying the conditioning voltage, the voltage dependencies of the availability of charge 1 as well as charge 2 were determined (Fig. 2).

The availability curve for charge 1 (Fig. 2, *open circles*) was well described by the sum of two Boltzmann terms and a constant. Because of their relatively low density (0.1 to 0.3 per μm^2; Droogmans and Nilius, 1989), T-type Ca^{2+} channels are
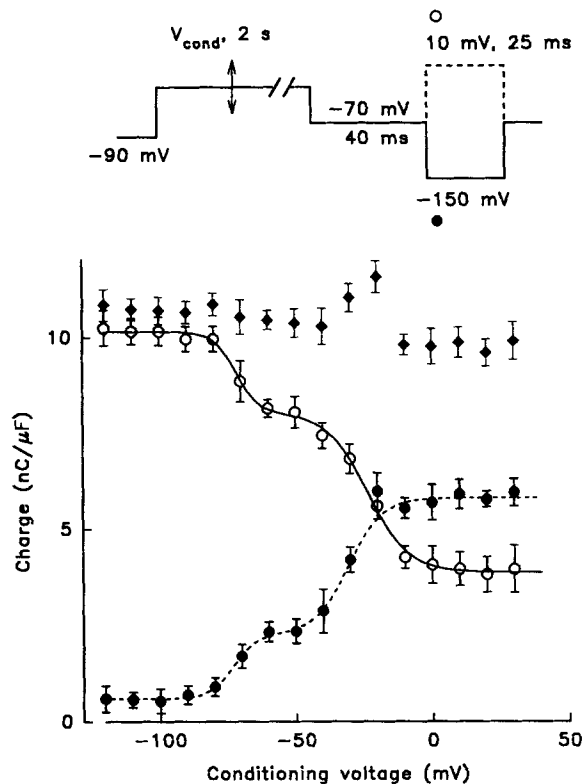

FIGURE 2. Availability curves of charge 1 (*open circles*) and charge 2 (*filled circles*). Conditioning pulses (2 s) to different voltages were applied before the 25-ms long test pulse from −70 to 10 mV to measure charge 1, or before the test pulse from −70 to −150 mV to measure charge 2. Both sets of data were obtained from the same three cells. The sum of charge 1 and charge 2 at each conditioning voltage is represented by filled diamonds. Data fitted by the equations:

$$Q_1 = 3.88 + 2.14/\{1 + \exp[(V + 71.6)/4.19]\} + 4.13/\{1 + \exp[(V + 23.5)/7.43]\}$$

$$Q_2 = 0.58 + 1.68/\{1 + \exp[(-V - 73.2)/4.41]\} + 3.54/\{1 + \exp[(-V - 30.8)/6.23]\}$$

Units are nC/μF and mV. The point Q_2(−20 mV) was omitted from the fit.

expected to make a very small contribution to charge movement in guinea pig ventricular myocytes (<0.05 nC/μF). Thus, the charge movement from other than Na^+ and L-type Ca^{2+} channels may be insignificant. As argued before (Bean and Ríos, 1989; Hadley and Lederer, 1989), the first term, centered at ~ −75 mV, is in all

likelihood associated with Na^+ channels, and the second term, centered at ~ -25 mV, arises from L-type Ca^{2+} channels.

The availability of charge 2 measured on the same cells at the same time, was fitted by the sum of two Boltzmann terms and a constant (Fig. 2, *filled circles*). These Boltzmann terms were almost identical in magnitude and steepness to the corresponding terms in charge 1. These data strongly imply that the Boltzmann components in charge 2 are also associated with Na^+ and L-type Ca^{2+} channels, and that voltage-dependent inactivation involves similar mechanisms of charge 1 to charge 2 interconversion in both types of channels.
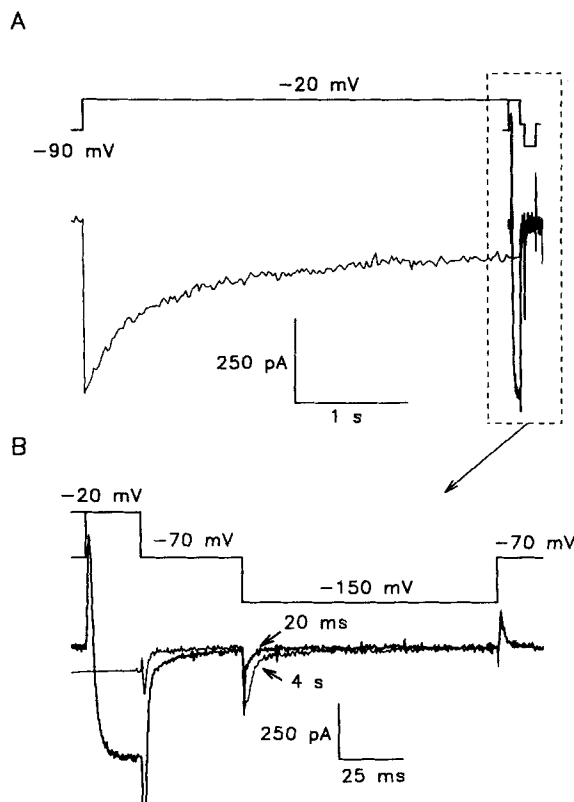
A

FIGURE 3. Simultaneous measurement of ionic current and charge 2. (*A*) Barium currents evoked by 3.9 s (*thin line*) or 20 ms (*thick line*) pulses to −20 mV, followed by a pulse from −70 to −150 mV to measure charge 2. At the transition to −70 mV the sampling rate was switched to 0.2 ms for both records. (*B*) Last 0.2 s of the records in *A*. Note that ionic current turned off completely during the gap at −70 mV even after the 20 ms pulse. Cell A2312C42, C_M = 165 pF, R_S = 3 MΩ.

The sum of charge 1 and charge 2 available (Fig. 2, *filled diamonds*) remained essentially constant as the conditioning voltage changed. The slight reduction of the sum at high depolarization may simply indicate that the step to −150 mV was not big enough to mobilize all available charge 2.

Charge 2 Can Be Measured Without Blocking the Ionic Current

Charge 2 moves at voltages where there is no measurable ionic current. This allowed us to apply the same protocol, used in the previous section, to measure charge 2 in external solutions without channel blockers. In that way it was possible to monitor charge 2 and ionic currents in the same solution. Fig. 3 represents an example using
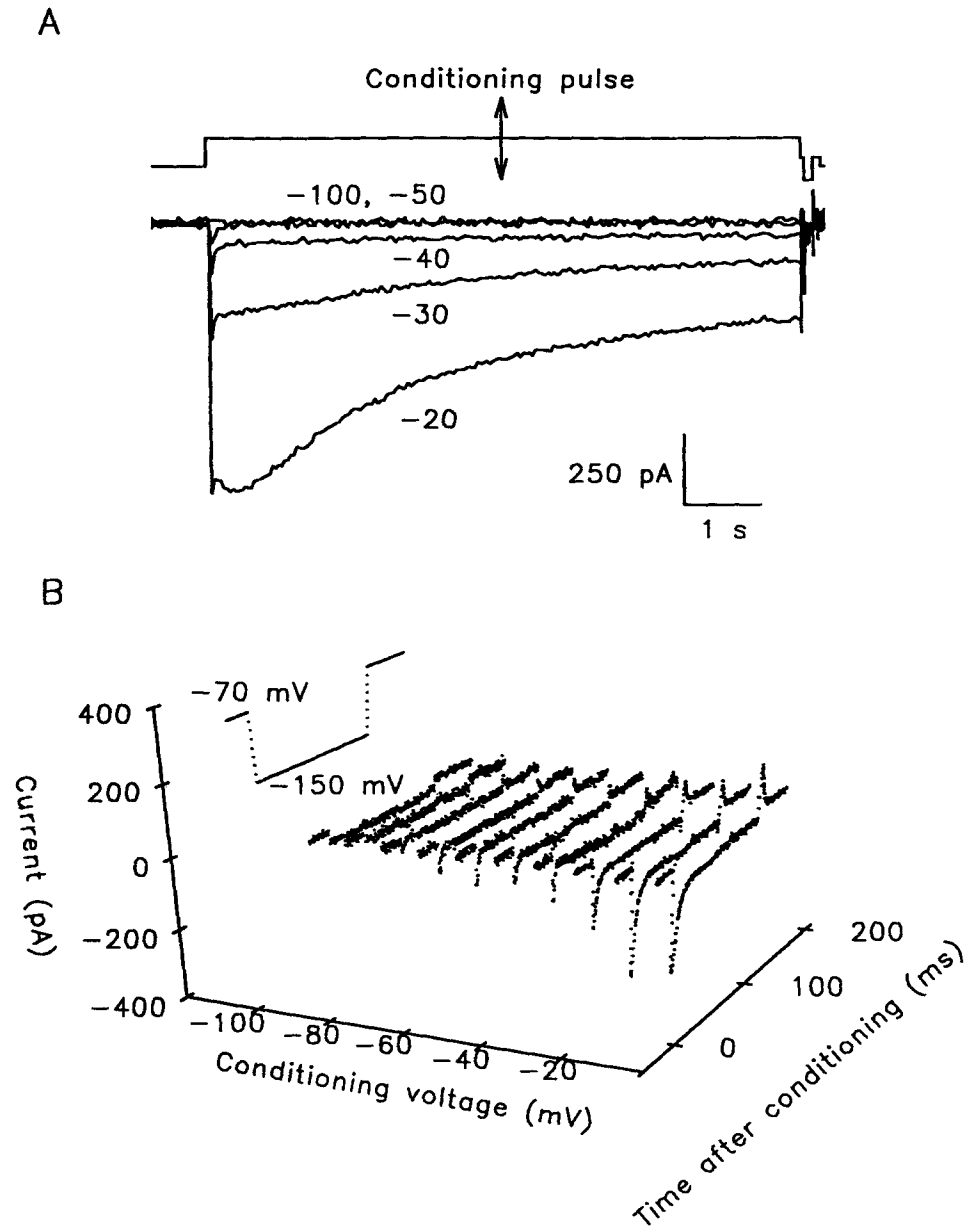
A

B

FIGURE 4. Charge 2 transients after conditioning pulses of different voltage. (*A*) Ba²⁺ currents elicited by conditioning pulses to voltages indicated in mV. Each pulse was followed by a step from −70 to −150 mV to measure charge 2 (note end of voltage protocol at top). (*B*) Charge 2 transients (last 0.2 s of records in *A*) plotted as a function of conditioning voltage. Cell 92423C10, C_M = 189 pF, R_S = 1.3 MΩ.

Barium external and *BAPTA* internal solutions. The pulse from h.p. to −20 mV evoked Ba^{2+} currents. In Fig. 3 *A* two current traces obtained with pulses of different duration are superimposed so that the ends of the pulses coincide. The record in thin trace was obtained with a 4-s pulse, the other with a 20 ms depolarization to −20 mV. After a gap at −70 mV the voltage was stepped to −150 mV, to measure charge 2.
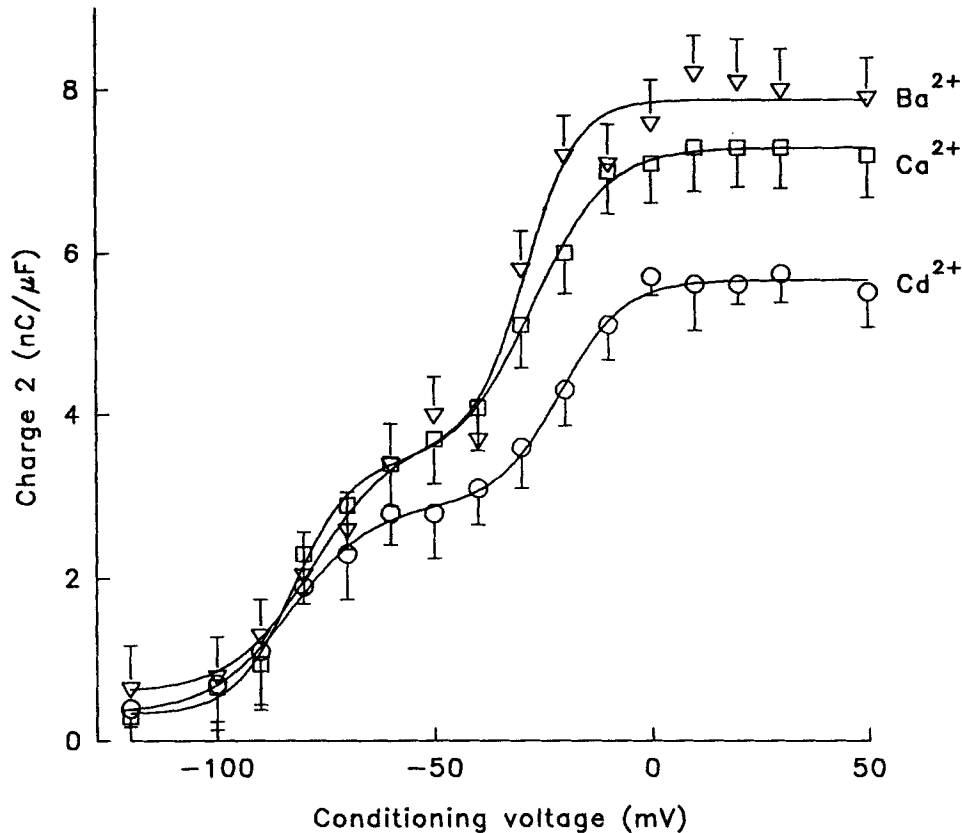

FIGURE 5.   Availability curves of charge 2 obtained in the presence of different metal cations. External solutions were *Barium* (*triangles*), *Calcium* (*squares*) and *Cadmium* (*circles*). All solutions were applied in the same four cells. Data fitted by equation:

$$Q_2 = Q_0 + Q_{Na}/\{1 + \exp[(V_{Na} - V)/K_{Na}]\} + Q_{Ca}/\{1 + \exp(V_{Ca} - V)/K_{Ca}]\}.$$

Best fit values of parameters are listed in Table II.

Fig. 3 *B* represents the last 0.2 s of the traces in *A* on an expanded time scale. The longer conditioning pulse (*thin trace*) produced more inactivation of the ionic current and more charge 2 than the shorter one.

The availability of charge 2 also depended on the conditioning voltage. One experiment is illustrated in Fig. 4. Panel A shows a set of Ba^{2+} currents evoked by 7.8

s (conditioning) pulses to different voltages. Each conditioning pulse was followed by a pulse to -150 mV to monitor charge 2. Ionic currents recorded in *Barium* solution often had a small peaky component that started to activate at -50 mV. At voltages more positive than -40 mV, this current was followed by a much larger, slowly decaying current. The early component of the ionic current is presumably through T-type Ca^{2+} channels (Bean, 1985) that represent a small fraction of Ca^{2+} channels in guinea pig ventricular myocytes (Balke, Rose, Marban, and Wier, 1992).

The asymmetric currents evoked by the step to -150 mV are plotted in Fig. 4 *B*. The current traces are stacked in three dimensions as a function of the conditioning voltage. Focusing on the early peaks during the ON, two components are clearly seen in the dependence of the availability on conditioning voltage. The first component was detectable after conditioning to -100 or -90 mV and saturated at ~ -50 mV. The second component, of greater amplitude, appeared after conditioning at higher voltages and saturated at positive voltages.

TABLE II

Two-Boltzmann Fits to Availability of Charge 2 in Different External Solutions

External solution	Q_0	V_{Na}	K_{Na}	Q_{Na}	V_{Ca}	K_{Ca}	Q_{Ca}
	$nC/\mu F$	mV	mV	$nC/\mu F$	mV	mV	$nC/\mu F$
Barium	0.62 (0.37)	-77.9 (5.5)	9.1 (5.0)	3.07 (0.84)	-28.9 (2.6)	5.9 (2.1)	4.19 (0.68)
Calcium	0.33 (0.12)	-82.5 (1.4)	6.7 (1.2)	3.08 (0.23)	-27.2 (1.2)	8.5 (1.0)	3.88 (0.19)
Cadmium	0.35 (0.14)	-82.7 (2.0)	9.3 (1.9)	2.57 (0.24)	-20.9 (1.4)	7.4 (1.2)	2.74 (0.17)

ON charge moved by a pulse from -70 to -150 mV (Q_2) was fitted as a function of 7.8 s conditioning voltage (V) by:

$$Q_2 = Q_0 + Q_{Na}/\{1 + \exp[(V_{Na} - V)/K_{Na}]\} + Q_{Ca}/\{1 + \exp[(V_{Ca} - V)/K_{Ca}]\},$$

where Q_0 is a constant added to the fit, V_{Na}, K_{Na} and Q_{Na} are the parameters of the more negatively located component of availability (associated with sodium channels), V_{Ca}, K_{Ca}, Q_{Ca} are the parameters of the component associated with calcium channels.
In parentheses are the SEM values ($N = 4$).

Charge 2 Depends on the External Cations

The above measurements was carried out in *Barium*, *Calcium*, and *Cadmium* external solutions in the same cells (dialyzed with *BAPTA* internal solution). The individual availability curves were averaged over four cells and are plotted in Fig. 5. The best fit parameters of two Boltzmann components are listed in Table II.

In *Barium* the total charge 2 available was about 10–15% greater than in *Calcium*. Most of the difference is in the more positively distributed component (Q_{Ca}). Additionally, we found a small increase in Q_0, the charge moved in the range of charge 2, even after conditioning at very negative voltages. This component, which was more pronounced in *Barium*, may be charge 1 of Na^+ channels. In *Cadmium*, both components of charge 2 (Q_{Na} and Q_{Ca}) were reduced by 20–30%.

The Availability of Charge 2 Does Not Depend on Ca^{2+} Current

Ca^{2+}-dependent inactivation was studied by measuring the availability of charge 2 and ionic current. This was done in *Calcium*, in cells dialyzed with an internal solution containing 0.5 mM EGTA, a relatively low buffer concentration. In these conditions Ca^{2+} currents inactivated very rapidly, the main component of decay having a time constant of less than 20 ms. This inactivation was due to internal Ca^{2+}, as demonstrated by the characteristic dependence of I_{Ca} on the voltage of a conditioning pulse (I_{Ca} availability curve). One experiment is illustrated in Fig. 6. The prepulse to 20 mV, producing the greatest Ca^{2+} current, caused the greatest reduction of the test current (A).
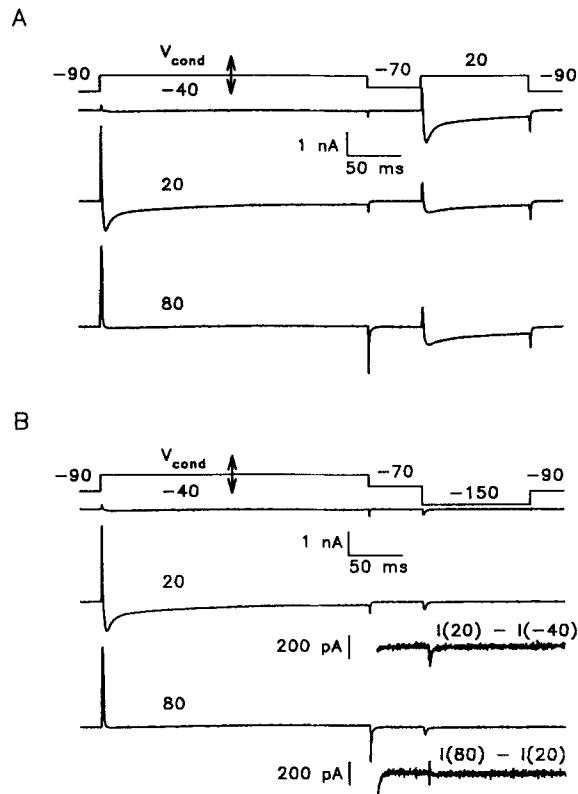

FIGURE 6. Effects of conditioning on I_{Ca} and charge 2. (A) Ca^{2+}-dependent inactivation of I_{Ca} in a double-pulse experiment (protocol at top, voltages listed in mV). The test current after conditioning to 80 mV was greater than after conditioning to 20 mV. (B) Charge 2 measured in the same conditions in the same cell. The noisy traces are differences between charge 2 currents as indicated. Internal solution, *EGTA*. External solution, *Calcium*. Cell 920102C22, C_M = 150 pF, Rs = 5.4 MΩ.

Following a similar procedure as in the previous study of voltage-dependent inactivation, it was possible to measure the amount of charge 2 available in the same solutions for recording I_{Ca}. The result is illustrated in B. The conditioning pulse to 20 mV, which elicited the greatest I_{Ca}, did not induce more charge 2 than the conditioning pulse to 80 mV, during which less Ca^{2+} entered the cell.

Data from four similar experiments are summarized in Fig. 7. The upper panel represents the availability of charge 2 (*circles*) and I_{Ca} (*triangles*) measured during the test pulse, as a function of conditioning pulse voltage. The lower panel plots the peak
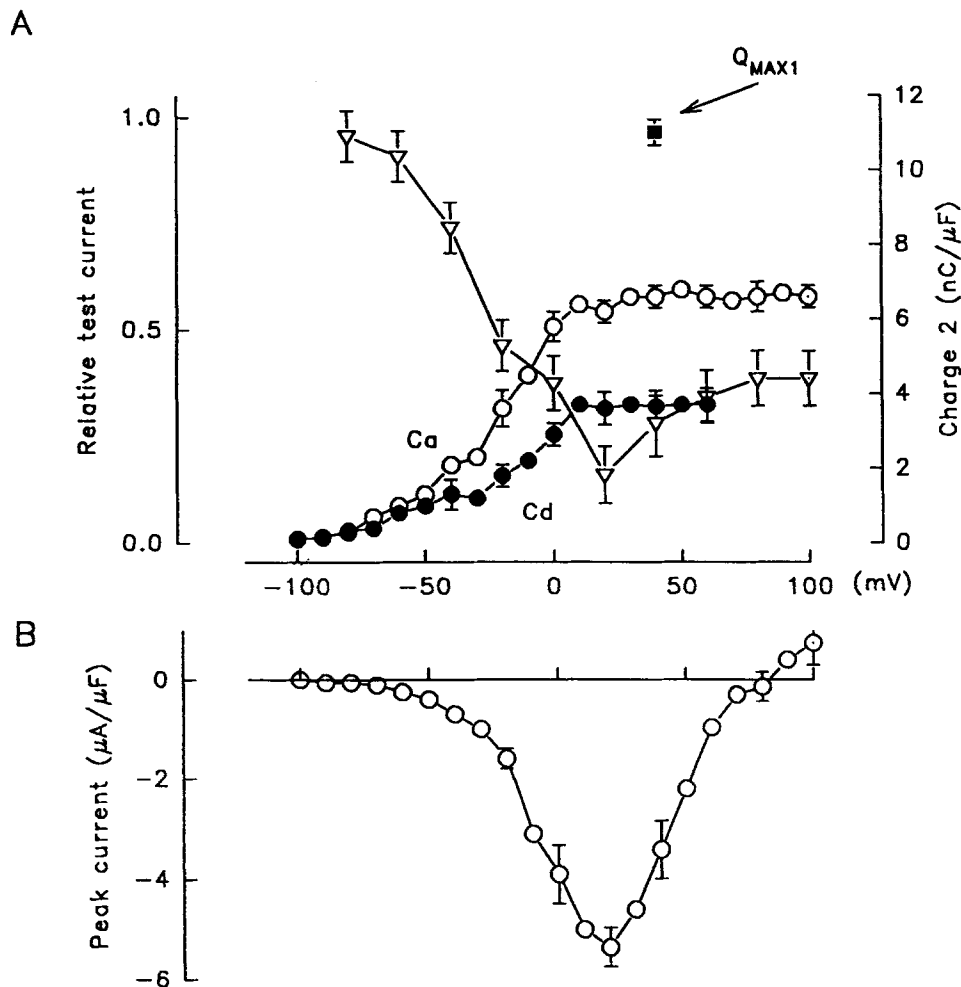
A

B

FIGURE 7. Peak I_{Ca} and availability of I_{Ca} and charge 2. Data from four cells, pulse protocols illustrated in Fig. 6. (*A*) Availability curves for I_{Ca} (*open triangles*) and charge 2 measured in *Calcium* (*open circles*) or *Cadmium* (*filled circles*). The plots were scaled so that the maximum availability of I_{Ca} (at -90 mV) coincided with the maximum of charge 1 (Q_{max1}) measured in *Cadmium* solution by a pulse from -110 to 40 mV. (*B*) Peak I_{Ca} measured during conditioning pulses to the voltages in the abscissa.

I_{Ca} *vs* voltage relationship in the conditioning pulse. The upper panel shows that the test I_{Ca} had a pronounced minimum at 20 mV, precisely the voltage that elicited the largest Ca^{2+} current during conditioning. However, the amount of charge 2 only increased with conditioning voltage. The maximal charge movement in polarized cells was measured by a voltage step from h.p. to 40 mV and is represented by the filled square. The extent of inactivation of the ionic current (complement to 1 of the values represented by *triangles*) and the extent of charge 1 to charge 2 conversion (*circles*) were similar ($\sim 60\%$) at the highest conditioning voltages.

The upper panel gives another illustration of the dependence of charge 2 on the external cation. While the open symbols represent data obtained in *Calcium*, the filled circles average data obtained (later in the same cells) in *Cadmium*. The availability of charge 2 had the same monotonic dependence on conditioning voltage but saturated at only ~60% of the maximum in *Calcium*. This reduction of charge 2 by Cd^{2+} is greater than in the experiments illustrated in Fig. 5, mainly because the conditioning pulses were much longer in those experiments (4 s) than in the ones represented in Fig. 7 (0.25 s). Because Cd^{2+} slows the onset of charge 2 in addition to changing steady-state availability, the difference is greater at shorter times of conditioning.

DISCUSSION

Interconversion of Charges 1 and 2

Prolonged depolarization inactivates channels and shifts the voltage distribution of charge movement to negative voltages in axonal Na^+, and skeletal and cardiac Ca^{2+} channels (Bezanilla et al., 1982; Brum and Ríos, 1987; Shirokov et al., 1992). The present results demonstrate that reduction of the charge available at voltages where the channel activates (charge 1) is accompanied by increase of the charge at very negative voltages (charge 2). The sum of charge 1 and charge 2 remains essentially constant after any conditioning.

This observation is in good agreement with the formalism developed for charge 1–charge 2 interconversion in skeletal muscle (Brum and Ríos, 1987). In more molecular terms, it means that the voltage dependent inactivation of the L-type cardiac Ca^{2+} channel is accompanied by a change in the environment of the voltage sensing portions of the channel. These alterations are very specific: of the three parameters in the Boltzmann description only the transition voltage changes. This means that the chemical free energy of interaction of sensors and environment changes. The total mobile charge, however, is conserved, implying that the product of charge on the sensors and the fraction of electric field traversed does not change upon inactivation. This in turn strongly implies that the charge on the sensors does not change and that the sensors move between the same initial and final stable positions in the membrane regardless of the ability of the channel to open.

The most striking feature of the availability curve of charge 2 measured here is that it has two Boltzmann components analogous to those of the dependence of charge 1 on the conditioning voltage (Bean and Ríos, 1989; Hadley and Lederer, 1989; Shirokov et al., 1992). In these experiments, charge 1 was measured by a test pulse to a voltage that activates ionic currents (say 0 mV). Conditioning depolarizations up to −50 mV caused reduction of charge 1, mostly due to inactivation of Na^+ channels. The component lost after conditioning to higher voltages is related to inactivation of Ca^{2+} channels. The existence of separate components in the availability curve of charge 2 implies that after prolonged depolarization the gating charge of Na^+ channels does not immobilize but shifts its voltage distribution to negative voltages, as is the case with Ca^{2+} channels. In other words, inactivation of cardiac Na^+ channels involves charge 1–charge 2 interconversion.

Charge 2 of Ca^{2+} channels (but not Na^+ channels) is greater in external Ba^{2+} than in external Ca^{2+}. Cd^{2+}, however, reduces substantially the amount of charge 2 of

both Na^+ and Ca^{2+} channels, both because it slows its onset and reduces its steady state availability. This presumably means that in Cd^{2+}, channels inactivate more slowly and to a lesser extent. It has been shown (Pizarro, Fitts, Uribe, and Ríos, 1989) that the presence of metal cations in the external solution stabilizes the skeletal muscle VSECC in its charge 1 form. The present results are consistent with these observations and underscore the fundamental similarity between the two voltage-operated, dihydropyridine-sensitive molecules.

The measurement of charge 2 with a pulse from -70 to -150 mV relied on its characteristic voltage dependence. This may not be entirely adequate for Na^+ channel gating current, which moves at more negative potentials than Ca^{2+} channel gating current. Thus, the charge movement observed at -70 mV, at the OFF of the pulse to -150 mV (Fig. 3 *B*), could be charge 1 of Na^+ channels. This small charge movement is not charge 2 because it is about the same after the long conditioning that greatly increases charge 2 at the ON.

Ca-dependent Inactivation and Interconversion of Charge

Current-dependent inactivation of Ca^{2+} channels is thought to involve either direct binding of Ca^{2+} to a receptor site on the channel and its closing by an allosteric mechanism or Ca^{2+}-dependent dephosphorylation of the channel (Eckert and Chad, 1984). Hadley and Lederer (1991) studied the effect of a change in the intracellular free Ca^{2+} concentration on the availability of Ca^{2+} channel gating currents in ventricular myocytes. Depending on the nature of the photolabile Ca^{2+} chelator, flash photolysis of caged calcium could produce either facilitation or inhibition of cardiac Ca^{2+} currents, but it had no obvious effect on gating currents.

In previous work (Shirokov et al., 1992) we presented evidence that the gating charge of L-type Ca^{2+} channels undergoes charge 1 to charge 2 interconversion upon voltage-dependent inactivation of the channels. Now we show that this interconversion does not happen when the inactivation is due to Ca^{2+} entry. This result may be interpreted in two very different ways.

The more straightforward interpretation is that there is no Ca^{2+}-dependent charge interconversion in any of the channels. In other words, inactivation caused by entry of Ca^{2+} is not accompanied by the changes in charge movement associated with voltage-dependent inactivation.

There is another possibility. The magnitude of charge movement is disproportionately large compared with the estimates of density of I_{Ca} channels (Bean and Ríos, 1989). One interpretation is that only a minor fraction of DHP-receptors constitute functional channels. If Ca^{2+}-dependent inactivation was strictly local (affecting only the channels that pass current, as suggested by Yue, Backx, and Imredy, 1990), this inactivation could be accompanied by charge interconversion, and go undetected due to the small number of channels involved.

Assuming that gating charge movement corresponds to the transfer of 10 elementary charges per channel, the contribution of two functional channels per μm^2 (Rose, Balke, Wier, and Marban, 1992) is ~ 0.5 nC/μF. If one half of these channels are inactivated by Ca^{2+} (Rose et al., 1992), then the expected increase in charge 2 after conditioning at voltages of maximal current would be ~ 0.2 nC/μF. This value, approximately equal to the standard error of the measurement, would have been

detected in averages. Of course, this reasoning depends on unproven assumptions regarding channel density and gating charges per channel.

To help decide between these two possibilities, we built a model of Ca^{2+} channel gating based on our first interpretation, that charge interconversion does not accompany Ca^{2+}-dependent inactivation. Since the interpretation implies that the channel closure by Ca^{2+} is entirely independent from the voltage driven mechanisms, the model postulates two independent inactivation mechanisms. Extremely simple by design, the model reproduces many properties of the macroscopic current and even some observations at the single channel level. It constitutes indirect evidence in favor of our first interpretation.

Model

The equations and parameter values are given in the Appendix. The model is based on two assumptions, illustrated in the cartoon (Fig. 8): (a) A four-state kinetic scheme describes voltage-dependent activation and inactivation of channels. Transitions of voltage-dependent activation and inactivation do not depend on $[Ca^{2+}]_i$. This scheme, involving two gates (1 and 2), is analogous to one introduced by Brum and Ríos (1987) for the VSECC of skeletal muscle. (b) A third process (gate 3 in the cartoon) is Ca^{2+}-sensitive. The gate is normally open ~ 10% of the time and closes further when Ca^{2+} binds to its controlling site. The local $[Ca^{2+}]$ is determined by the flux of Ca^{2+} from the mouth of the channel, being high when the channel is open and low otherwise. This ignores any contribution from the sarcoplasmic reticulum, an oversimplification supported by the fact, discussed later, that the model works well only if the controlling site is placed very close to the channel mouth.

Transitions of gate 1 depend only on membrane voltage. Gate 2 (voltage dependent inactivation) is coupled to gate 1 (its transition rate constants depend on the state of gate 1). As described before for L-type channels (Shirokov et al., 1992) and voltage sensors of skeletal muscle (Brum and Ríos, 1987), transitions due to gates 1 and 2 are related as follows:
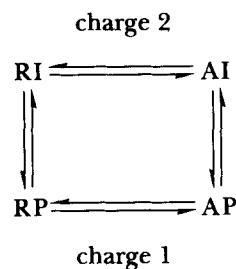
charge 2

$$
\begin{array}{ccc}
RI & \rightleftharpoons & AI \\
\updownarrow & & \updownarrow \\
RP & \rightleftharpoons & AP
\end{array}
$$

charge 1

DIAGRAM I

Individual letters represent states of individual gates. The activationgate, directly operated by voltage, makes transitions between states R (resting) and A (active). In currently favored molecular pictures (Guy and Seetharamulu, 1986; Catterall, 1988) these states may correspond to situations with all S4 segments in resting or activating positions.

An inactivation gate undergoes transitions between states P (primed) and I (inactivated). To justify the observations on charge interconversion, when the model channel becomes inactivated, the voltage distribution of charge movement is shifted negatively. As first suggested by Bezanilla et al., (1982) to explain similar effects of
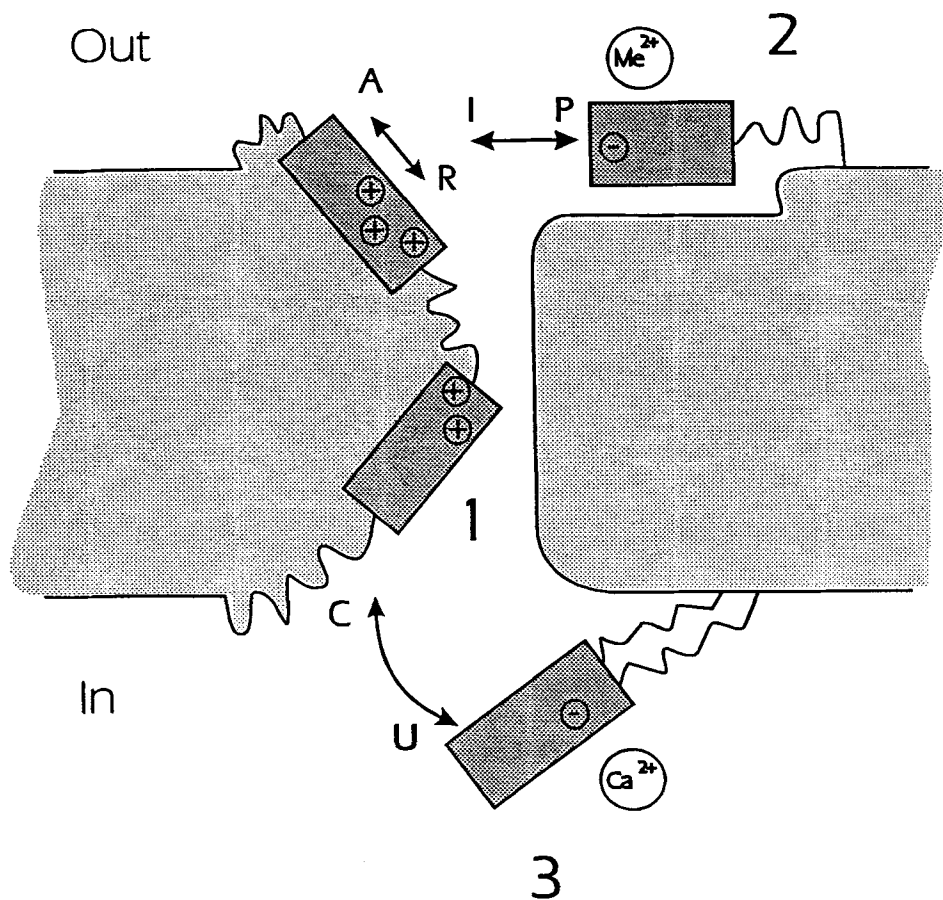

FIGURE 8. Cartoon of the model of Ca^{2+} channel gating described in the text. Three two-state gates are indicated: gate 1 represent voltage-dependent activation. Gate 2 causes "voltage-dependent" inactivation; the antagonization of voltage-dependent inactivation by extracellular metal ions is represented by an ion binding site on the gate. Gate 3, representing Ca^{2+}-dependent inactivation, has a Ca^{2+} binding site and strongly favors state C when the site is occupied. Gates 1 and 2 are interdependent, their states are represented by diagram 1 in the text. The states of gate 3 and Ca^{2+} binding are represented by diagram 2.

inactivation in squid axon Na$^+$ channels, the phenomenon may be envisioned mechanistically as an attraction between voltage sensing segments and a hypothetical particle responsible for voltage-dependent inactivation (cartoon). In thermodynamic terms, to move charge in inactivated channels the external electric field has to do

more work (~ 5 $k_B T$, given a -80 mV shift in transition voltage and 15 mV steepness factor)[1].

The four-state diagram 1 describes well the charge movement in cardiac myocytes (Shirokov et al., 1992). Rapid ($\tau \simeq 3$ ms) voltage dependent transitions A$\leftrightarrow$R underlie charge 1 and charge 2, and slower ($\tau \simeq 200$ ms) I$\leftrightarrow$P transitions determine their interconversion.

Gate 3 is responsible for Ca^{2+}-dependent inactivation. Its rate constants only depend on whether a regulatory site is bound to or free from Ca^{2+}. This Ca^{2+}-dependent gate makes transitions between the two states: C ("covered") and U ("uncovered"). When calcium binds, the covered state becomes more probable.

$$Ca^{2+}\diagdown \qquad C \rightleftharpoons U \qquad \diagup Ca^{2+}$$
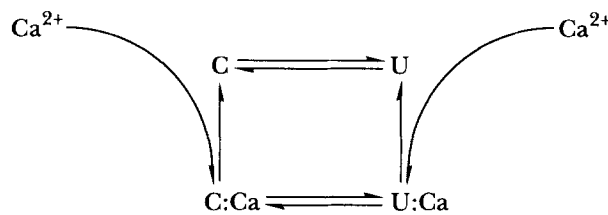$$C:Ca \rightleftharpoons U:Ca$$

DIAGRAM II

The $C \Rightarrow U$ transition proceeds at a slow rate even when there is no Ca^{2+} bound at the regulatory site (therefore, channels that are fully activated by voltage will open sparingly). When Ca^{2+} binds, the covered state is favored even more. This is accomplished in the model by making the $C:Ca \Rightarrow U:Ca$ rate constant smaller than $k_{C,U}$.

With these assumptions, even though the Ca^{2+}-dependent gate does not depend explicitly on any other process, it becomes coupled to the other gates. The local $[Ca^{2+}]$ determines the rates of gate 3 transitions, and is in turn determined by the collective state (open or close) of the channel[2].

Let the collective states of the channel be represented by three letters. Thus APU and APU:Ca represents the only open states. If the gates were strictly independent, the channel P_0 (sum of the probabilities of APU and APU:Ca) would simply be the product of the occupancies of the permissive states in diagrams 1 and 2. Because this was not the case, a kinetic scheme including all possible states had to be solved. The total number of states (combinations of four two-state processes) is sixteen. In spite of the multiplicity of states, the essential qualitative aspects of the model are easy to comprehend.

---

[1] The voltage distribution of charge movement is less steep than the availability curves of charge 1 and charge 2. In the model, this would happen if the $P \leftrightarrow I$ transition required the movement of multiple activating particles. In terms of recent molecular models, this would be the case if voltage dependent inactivation was linked to transitions of several S4 segments, in a manner similar to what is thought about channel activation.

[2] Additionally, the fact that $I \times r$ drops are taken into account to determine the actual transmembrane voltage, brings about another form of coupling among gates. The transmembrane voltage affecting the voltage dependent rates of gate 1 is a function of the applied voltage and the open or close state of the channel.

The following description applies when the values of kinetic constants are those given in the Appendix. At rest, gate 1 is in state R, gate 2 is in state P, and gate 3 is in state C in about 90% of the channels. When a depolarizing pulse is applied, gate 1 goes to state A, but only the few channels whose Ca^{2+}-dependent gate is in state U open (joint state APU). Opening causes the increase of $[Ca^{2+}]$ at the regulatory site (a fast process, see Appendix), and the binding that ensues favors state C:Ca, then C as $[Ca^{2+}]$ decays rapidly upon channel closure. The joint state is then APC, from which the channel can reopen. Voltage dependent inactivation corresponds to transitions to the more stable closed state AI.

To specify the four-state diagram 2, values of dissociation constants are needed. A $[Ca^{2+}]_i$ of 0.1 μM has been reported to reduce I_{Ca} by $\simeq 50\%$ in different tissues (Byerly and Moody, 1984; Dupont, Bossu, and Feltz, 1986; Ohya, Kitamura, and Kuriyama, 1988). Buffering of intracellular calcium to lower concentrations eliminates fast inactivation of I_{Ca} in cardiac myocytes (Bechem and Pott, 1985). This sets the K_D of covered channel sites at $\simeq 0.1$ μM.

Because Ca^{2+} binding enhances the stability of state C, microscopic reversibility requires that the affinity for Ca^{2+} of state C be much higher than that of U. As argued above, channels in state C:Ca essentially do not uncover. Therefore the $[Ca^{2+}]_i$ that causes half saturation of the channels in state C will also reduce, by the same factor, the equilibrium occupancy of state U. This means that the K_D of state C for Ca^{2+} is approximately the concentration that reduces I_{Ca} by 50%.

From these considerations the dissociation constant of C:Ca was set to 0.05–0.1 μM and that of U:Ca was made 100-fold greater. This implies that $[Ca^{2+}]$ at the control site has to be at least tens of μM to close the channel. As shown in the Appendix, such concentrations can be reached only at very short distances from the mouth of the channel.

This conclusion is in agreement with recent experimental evidence. Ca^{2+}-dependent inactivation was reported in studies of cardiac Ca^{2+} channels in lipid bilayers (Rosenberg and Haack, 1993). It was also observed in *Xenopus* oocytes expressing $\alpha 1$ and $\beta 2$ subunits or a COOH terminus deletion mutant of the $\alpha 1$ subunit (Neely, Wei, Birnbaumer, and Stefani, 1993). These data suggest that Ca^{2+}-dependent inactivation is a property of the $\alpha 1$ subunit.

In apparent contradiction, block of the snail *Lymnaea stagnalis* Ca channels by photoreleased internal Ca was consistent with K_D in the submicromolar range (Johnson and Byerly, 1993). Because in this work photoreleased Ca^{2+} probably bound mostly to closed Ca^{2+} channels (state C in our model) the K_D found is consistent with our assumptions.

The present model belongs to a class in which Ca^{2+} binding directly affects a gating process. As indicated above, microscopic reversibility necessarily dictates that the Ca^{2+} binding affinity of the controlling site will depend on the gating state. This feature helps solve a contradiction, pointed out for instance by Kostyuk (1984). The estimates of affinity of the binding site based on modifications of internal $[Ca^{2+}]$ suggest a $K_D \simeq 10^{-7}$ M. The presence of a high affinity binding site in the pathway would reduce the open channel current substantially below observed values. For this reason, more complicated, indirect mechanisms of Ca^{2+}-dependent inactivation have

been considered, involving biochemical processes (Eckert and Chad, 1984). However, the K_D of a directly modulating binding site as described in the model, would increase 100-fold or more upon channel opening, thus reducing the interference with permeation, even if the binding site is within the permeation pathway.
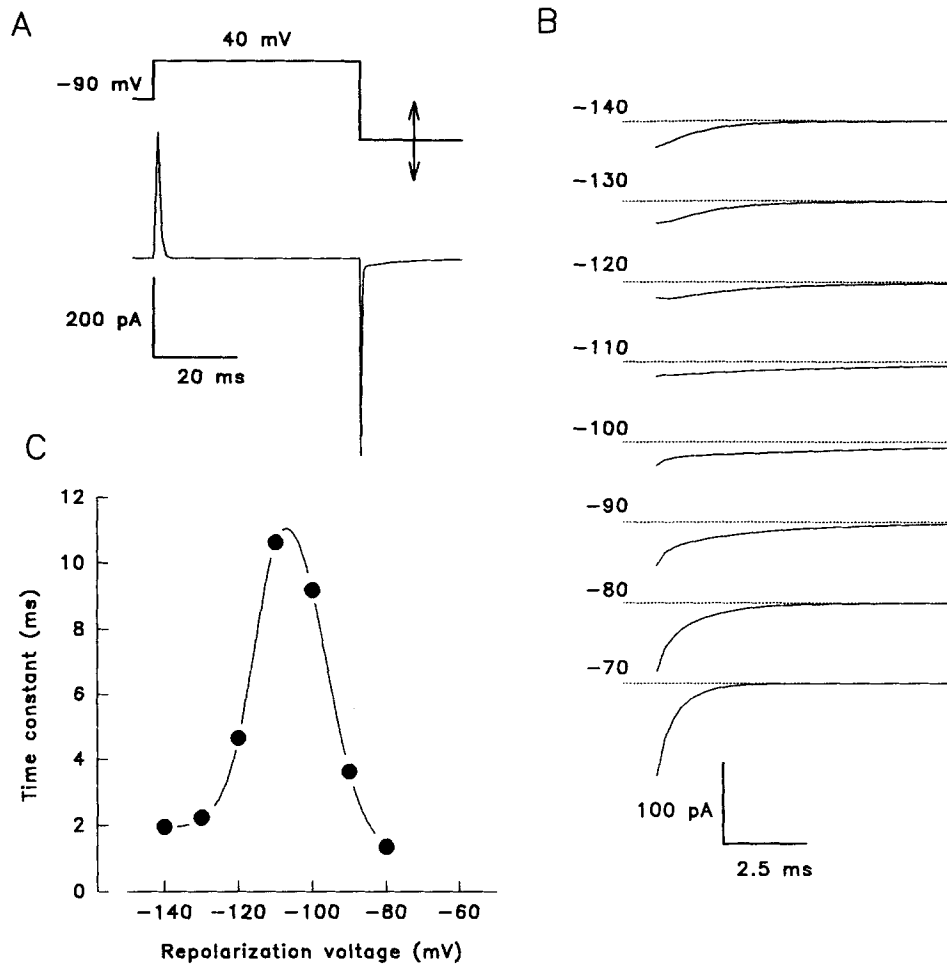

FIGURE 9. Simulations of charge movement. (A) Simulated charge movement elicited by the pulse shown (repolarization to −100 mV). Note the slow component at the OFF. (B) Slow components of the OFF at different repolarization voltages, elicited with the pulse protocol shown in A. First 1.5 ms of transient were blanked. (C) Time constants of a single exponential fit to the slow component vs repolarization voltage.

Simulations

First, we show how the model simulates charge movement (setting to zero the single-channel current). Hadley and Lederer (1989) and Shirokov et al. (1992) found that the OFF transient of charge movement has a slow component at negative

voltages. Based on several properties of this current, including the bell-shaped dependence of its time constant on repolarization voltage, Shirokov et al. (1992) concluded that it is charge moving among inactivated states (charge 2). These features are reproduced in the simulations, as shown in Fig. 9. *A* shows the voltage protocol and an example of simulated charge movement. The repolarization voltage
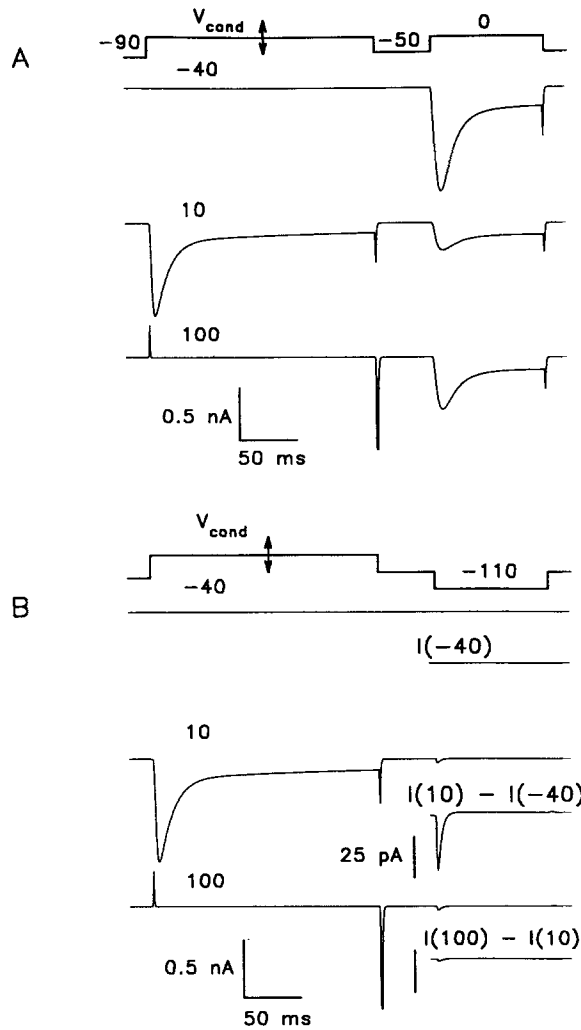

FIGURE 10. Simulations of double pulse experiments. Pulse protocols are at top of each panel (voltages listed in mV). Traces represent the sum of ionic and gating currents. (*A*) Test pulse to 0 mV, to activate I_{Ca} available after three different conditioning pulses. (*B*) Test pulse to −110 mV, to evoke charge 2 after the same conditioning protocols.

for this trace is −100 mV. At this voltage the slow component of charge movement is clearly seen, even after a relatively brief (50 ms) depolarization, as found experimentally (Shirokov et al., 1992). Simulated charge movement in OFFs from 40 mV to different repolarization voltages are plotted in *B*, blanking for clarity the fast component that moves during the first 1.5 ms of the transient. The time constants of

exponentials fitted to the slow component are plotted vs repolarization voltage in C. This dependence is similar to that measured experimentally (Figs. 9 and 10 of Shirokov et al., 1992).

Next, we examined the behavior of the model in the presence of Ca^{2+} current (and Ca^{2+}-dependent inactivation). We chose the rate constant of Ca^{2+} binding to the regulatory site to be 10^8 M^{-1} s^{-1}, which is close to the diffusion limit. The simulations of ionic and gating currents were almost identical to experimental traces if the distance between the channel mouth and the regulatory site was less than 10 nm.
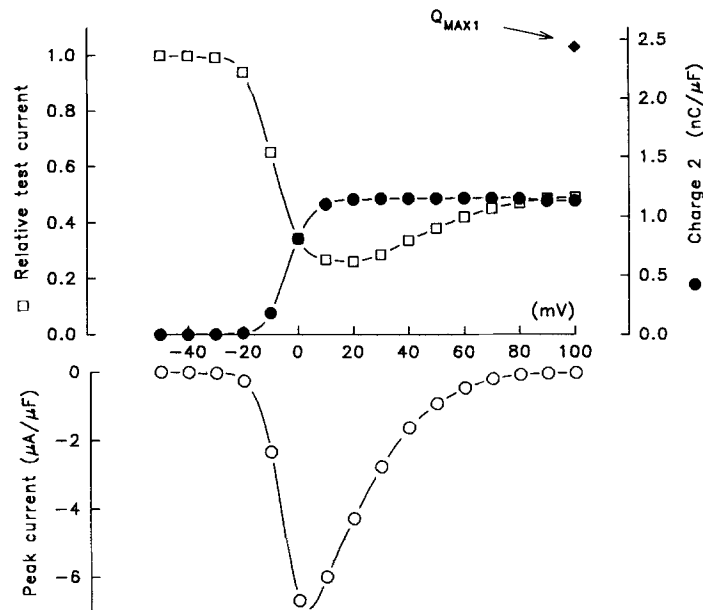

FIGURE 11. Simulated peak I_{Ca} and availability of I_{Ca} and charge 2. Summary of a series of simulations like the ones represented in Fig. 9. The open circles represent peak I_{Ca} as a function of test voltage (in unconditioned simulations). The open squares represent availability of I_{Ca}, that is, peak I_{Ca} for a test pulse to 0 mV, as a function of voltage of a conditioning pulse with the duration and placement described in Fig. 9. (*Filled circles*) Availability of charge 2 (evaluated in the simulations as charge moved by a pulse from −50 mV to −110 mV) as a function of conditioning voltage.

Fig. 10 illustrates the sum of ionic and gating currents simulated with the pulse protocols from the experiment in Figs. 6 and 7. The ionic current inactivates with two time constants (of ~20 and 200 ms). Inactivation is faster when the current is greater but its rate does not increase with voltage. When the amplitude of the conditioning current is greatest, the amplitude of the test current reaches a minimum.

A pulse to −100 mV evokes only charge 2 (panel B). This charge is slightly greater after conditioning to +100 mV (even though inactivation of the ionic current is less, as shown in A).

Fig. 11 illustrates similar calculations for different conditioning potentials. The simulated peak $I_{Ca}(V)$ and the availability curves for I_{Ca} and charge 2 reproduce well

the experimental results (Fig. 7). However, as others who assumed simple models have noted before (Bean and Ríos , 1989; Hadley and Lederer, 1989), the simulated charge movements are significantly smaller than those measured experimentally.

An interesting feature of this model is that the simulated tail currents are very fast, in fact they are limited by the speed of voltage clamp. This is the case for real currents (Bean, 1985; Campbell, Giles, Robinson, and Shibata, 1988). In the present model, closure upon repolarization is due to the voltage-dependent gate 1, whose rate constant is an exponential function of voltage. This feature cannot be reproduced by sequential schemes of the $C \leftrightarrow C \leftrightarrow O$ type, in which the last (opening) step is weakly voltage-dependent (Cavalie, Ochi, Pelzer and Trautwein, 1983). The essential difference between these two models is the possibility in the parallel model of closing the channel by three different processes.

This model also gives insights into the processes that determine the kinetics of inactivation. The normal pathway during a depolarizing pulse includes a voltage dependent activation step ($R \Rightarrow A$), whereby the channels that are previously uncovered become open. Then Ca^{2+}-dependent inactivation takes place. Because of the high $[Ca^{2+}]$ near the open channels, the rate of U to U:Ca transition is large (several ms^{-1}, cf Appendix). Therefore, the channels go rapidly into U:Ca and most of these close to C:Ca. In the simulations, this rate is ≈ 1 ms^{-1}. The speed of Ca^{2+}-dependent inactivation (of > 10 ms time constant in the simulations) is therefore not limited by either the Ca^{2+} binding step or the closure of Ca^{2+}-bound channels. It is the "uncovering" transition from C to U (with a rate constant of 0.1 ms^{-1}) that limits Ca^{2+}-dependent inactivation of the model channels.

APPENDIX

First we describe voltage dependent aspects, represented by state diagram 1, then Ca^{2+}-dependent inactivation (diagram 2), then the temporal and spatial dependence of the concentration of Ca^{2+} near an open channel.

The state of the model channel is designated as described in the text, by three letters, representing states of three gates, and a symbol for Ca^{2+} binding. Rate constants are represented by $k_{i,j}$, where i and j respectively represent the origin and destination states of the transition. Sixty four rate constants are needed to specify the model (four parallel processes, starting from each of sixteen states). However, assumptions of independence reduce substantially this number. These assumptions of independence are explicitly stated in equations 1 through 16 below. Thus, the voltage dependent rate constants governing gate 1 are entirely independent of gate 3 and Ca^{2+}:

$$k_{APC,RPC} = k_{APCCa,RPCCa} = k_{APU,RPU} = k_{APUCa,RPUCa} = k_{AP,RP}, \tag{1}$$

$$k_{AIC,RIC} = k_{AICCa,RICCa} = k_{AIU,RIU} = k_{AIUCa,RIUCa} = k_{AI,RI}, \tag{2}$$

$$k_{RPC,APC} = k_{RPCCa,APCCa} = k_{RPU,APU} = k_{RPUCa,APUCa} = k_{RP,AP}, \tag{3}$$

$$k_{RIC,AIC} = k_{RICCa,AICCa} = k_{RIU,AIU} = k_{RIUCa,AIUCa} = k_{RI,AI}, \tag{4}$$

Similar simplifications apply to the rate constants of voltage-dependent inactiva-

tion and repriming:

$$k_{APC,AIC} = k_{APCCa,AICCa} = k_{APU,AIU} = k_{APUCa,AIUCa} = k_{AP,AI},\qquad(5)$$

$$k_{AIC,APC} = k_{AICCa,APCCa} = k_{AIU,APU} = k_{AIUCa,APUCa} = k_{AI,AP},\qquad(6)$$

$$k_{RPC,RIC} = k_{RPCCa,RICCa} = k_{RPU,RIU} = k_{RPUCa,RIUCa} = k_{RP,RI},\qquad(7)$$

$$k_{RIC,RPC} = k_{RICCa,RPCCa} = k_{RIU,RPU} = k_{RIUCa,RPUCa} = k_{RI,RP},\qquad(8)$$

Eqs. 1–8 imply that gates 1 and 2 are interdependent, but independent from gate 3 and Ca^{2+}. Therefore, their function is described entirely by state diagram 1.

Because the measured time constants of charge movement or ionic current activation do not approach asymptotically zero at high voltages, the rate constants cannot simply be described by rates that depend exponentially on voltage. To limit the rate increase, the free energy difference between starting and transitional states was assumed to be a second order function of voltage (as done by Simon and Beam, 1985, in their study of the VSECC). Thus:

$$k_{RP,AP} = \alpha_1 \times \exp\{(V - V_1)/2K - b \times [(V - V_1)/2K]^2\},$$

$$k_{AP,RP} = \alpha_1 \times \exp\{-(V - V_1)/2K - b \times [(V - V_1)/2K]^2\},$$

$$k_{RI,AI} = \alpha_2 \times \exp\{(V - V_2)/2K - b \times [(V - V_2)/2K]^2\},$$

$$k_{AI,RI} = \alpha_2 \times \exp\{-(V - V_2)/2K - b \times [(V - V_2)/2K]^2\},$$

where $\alpha_1 = 0.2$ ms^{-1}, $\alpha_2 = 0.04$ ms^{-1}, $V_1 = 0$ mV, $V_2 = -80$ mV, $b = 0.1$ and $K = 4$ mV.

The inactivation rate constants were set to reproduce the time course of inactivation and the final level of inactivation at high voltage as:

$$k_{AP,AI} = 0.004 \text{ ms}^{-1},$$

$$k_{AI,AP} = 0.001 \text{ ms}^{-1},$$

The sum of the recovery rate constants $k_{RP,RI}$ and $k_{RI,RP}$ was set to 0.04 ms^{-1} to reproduce the kinetics of recovery at very negative voltages. Their ratio was derived from microscopic reversibility as:

$$k_{RI,RP}/k_{RP,RI} = (k_{AP,AI}/k_{AI,AP}) \times \exp[(V_1 - V_2)/K].$$

Due to the difference between V_2 and V_1 (the center voltages of charge 2 and charge 1) the above ratio is very large. This property, already noted for inactivation of the skeletal muscle VSECC, stresses that inactivation at high voltages and recovery at negative voltages proceed spontaneously, even though they do not have intrinsic voltage dependence, due to the large shift in voltage dependence between charges 1 and 2 (Brum and Ríos, 1987).

The simulations treated the channels as current sources generating both ionic and charge movement currents, in parallel with a linear capacitance $C_M = 150$ pF and in series with a resistance $R_S = 5$ MΩ. One equation described charging of the

membrane capacitance:

$$dV/dt = (V_f - V)/C_M R_S - (N/C_M) \times \{i(V) P_o + (k_B T/K)(dP_{AP}/dt + dP_{AI}/dt)\},$$

where V_f is applied voltage, N is number of channels, P_o is the open probability

$$P_o = P_{APU} + P_{APUCa},$$

$$P_{AP} = P_{APU} + + P_{APC} + P_{APUCa} + P_{APCCa},$$

$$P_{AI} = P_{AIU} + + P_{AIC} + P_{AIUCa} + P_{AICCa},$$

k_B — Boltzmann constant, T — absolute temperature.

The voltage dependence of the open channel current $i(V)$ was described by the constant field equation (Hodgkin and Katz, 1949) with $[Ca^{2+}]_i = 0$. The dependency of i on $[Ca^{2+}]_e$ was represented by a simple one site Ca^{2+} binding isotherm, with K_D of 14 mM (Tsien, Hess, McCleskey, and Rosenberg, 1987). The proportionality constant was set to have a unitary current of ~ 0.35 pA at 20 mV and saturating $[Ca^{2+}]_e$ (Yue et al., 1990). If $[Ca^{2+}]_e$ is in mM the unitary current in pA is

$$i(V) = \frac{0.08 \, V \exp(-V/12)}{(1 + 14/[Ca^{2+}]_e) [1 - \exp(-V/12)]},$$

and the total current through N channels is $N \times P_o \times i$. For calculations we used $[Ca^{2+}]_e = 10$ mM, giving a unitary current of 0.4 pA at 0 mV. The value of N was set at 375,000 which corresponds to 25 channels per μm^2.

Analogous assumptions of independence reduce the number of rate constants of gate 3 and Ca^{2+} binding to just those in state diagram 2. Namely, conversions among Ca^{2+}-free states:

$$k_{APC,APU} = k_{AIC,AIU} = k_{RPC,RPU} = k_{RIC,RIU} = k_{C,U}, \tag{9}$$

$$k_{APU,APC} = k_{AIU,AIC} = k_{RPU,RPC} = k_{RIU,RIC} = k_{U,C}, \tag{10}$$

conversions among Ca^{2+}-bound states:

$$k_{APCCa,APUCa} = k_{AICCa,AIUCa} = k_{RPCCa,RPUCa} = k_{RICCa,RIUCa} = k_{CCa,UCa}, \tag{11}$$

$$k_{APUCa,APCCa} = k_{AIUCa,AICCa} = k_{RPUCa,RPCCa} = k_{RIUCa,RICCa} = k_{UCa,CCa}, \tag{12}$$

and rate constants of Ca^{2+} binding and dissociation, which are only dependent on the state of gate 3:

$$k_{APC,APCCa} = k_{AIC,AICCa} = k_{RPC,RPCCa} = k_{RIC,RICCa} = k_{C,CCa}, \tag{13}$$

$$k_{APCCa,APC} = k_{AICCa,AIC} = k_{RPCCa,RPC} = k_{RICCa,RIC} = k_{CCa,C}, \tag{14}$$

$$k_{APU,APUCa} = k_{AIU,AIUCa} = k_{RPU,RPUCa} = k_{RIU,RIUCa} = k_{U,UCa}, \tag{15}$$

$$k_{APUCa,APU} = k_{AIUCa,AIU} = k_{RPUCa,RPU} = k_{RIUCa,RIU} = k_{UCa,U}. \tag{16}$$

The values of the rate constants in diagram 2 are:

$$k_{C,U} = 0.1 \text{ ms}^{-1},$$

$$k_{U,C} = 1 \text{ ms}^{-1}.$$

When Ca^{2+} is bound, the uncovering of the channel is more difficult:

$$k_{CCa,UCa} = 0.001 \text{ ms}^{-1},$$

$$k_{UCa,CCa} = 1 \text{ ms}^{-1}.$$

The rate constant of Ca^{2+} binding is assumed to be equal for both states U and C,

$$k_{C,CCa} = k_{U,UCa} = 10^8 \text{ M}^{-1} \text{ s}^{-1}.$$

The dissociation rate constant from state C:Ca is:

$$k_{CCa,C} = 0.005 \text{ ms}^{-1}.$$

The dissociation rate constant from state U:Ca is calculated from microscopic reversibility:

$$k_{UCa,U} = k_{CCa,C} \, k_{C,U} \, k_{UCa,CCa}/k_{U,C} \, k_{CCa,UCa} = 0.5 \text{ ms}^{-1}.$$

Because the local $[Ca^{2+}]$ participates in the differential equations it is necessary to describe the concentration near an open channel. Following ideas of Neher (1986) and Stern (1992), the local $[Ca^{2+}]_i$ is simulated as an instantaneous function of the current through the individual channel. The flux through the open channel is $i/2F$, where F is the faraday. If $[Ca^{2+}]_r$ is the concentration at rest (it was chosen to be 50 nM in the model), the concentration at time t and distance r from the mouth of a channel that opened at time 0 is:

$$[Ca] = [Ca]_r + \frac{i}{4\pi FDr} \, \text{erfc}\left(\frac{r}{2\sqrt{Dt}}\right),$$

where D is the diffusion coefficient of Ca^{2+} ($10^{-5} \text{ cm}^2 \text{ s}^{-1}$). The steady state concentration is

$$[Ca^{2+}]_{ss} = [Ca^{2+}]_r + i/4\pi FDr.$$

It is approximately equal (in μM) to $[Ca^{2+}]_r + 1,000 \times i/r$, when i is in pA and r in nm. For $i \simeq 0.1$ pA, $[Ca^{2+}]_{ss}$ at 10 nm will be 10 μM. Diffusion reaches steady state rapidly near the source. The *erfc* differs from its final value by less than 4% when the argument is less than 0.05, or t greater than 400 r^2/D. This means that the concentration profile reaches steady state in about 4 μs at $r < 10$ nm.

Different $[Ca^{2+}]$ drives the transitions depending on the state of the channel. The transitions in the open channel, that is from APU to APU:Ca, are driven by $[Ca^{2+}]_{ss}$. The transition rate is:

$$k_{U,UCa} \{[Ca^{2+}]_r + (i/4\pi FDr)\}.$$

For all other Ca^{2+}-free states AIU, RPU, RIU, APC, AIC, RPC, RIC, transitions to the corresponding Ca^{2+}-bound states are driven by $[Ca^{2+}]_r$.

The complete system consists of 15 independent differential equations describing transitions between 16 states, one equation of conservation of mass and one additional differential equation for voltage. It was solved by a fourth order Runge-Kutta routine (Press, Flannery, Teukolsky, and Vetterling, 1988). For the first voltage

step, the initial condition was the steady-state solution of the system at the holding potential. For all the following voltage steps, the initial condition was that reached at the end of the previous step.

REFERENCES

Armstrong, C. M. 1981. Sodium channels and gating current. *Physiological Reviews.* 61:644–683.

Armstrong, C. M., and F. Bezanilla. 1977. Inactivation of the sodium channels. II. Gating current experiments. *Journal of General Physiology.* 70:567–590.

Balke, C. W., and W. C. Rose, E. Marban, and W. G. Wier. 1992. Macroscopic and unitary properties of physiological ion flux through T-type Ca²⁺ channels in guinea-pig heart cells. *Journal of Physiology.* 456:247–265.

Bean, B. P. 1985. Two kinds of calcium channels in canine atrial cells. Difference in kinetics selectivity and pharmacology. *Journal of General Physiology.* 86:1–30.

Bean, B. P., and E. Ríos. 1989. Nonlinear charge movement in mammalian cardiac ventricular cells. Components from Na⁺ and Ca²⁺ channel gating. *Journal of General Physiology.* 94:65–93.

Benitah, J.-P., P. Bailly, J.-P. Da Ponte, C. Delgado, and P. Lorente. 1992. Slow inward current in pathological adult human ventricular cells. *Biophysical Journal.* 61:248a. (Abstr.).

Bezanilla, F., E. Perozo, D. M. Papazian, and E. Stefani. 1991. Molecular basis of gating charge immobilization in Chaker potassium channels. *Science.* 254:679–683.

Bezanilla F., R. E. Taylor, and J. M. Fernandez. 1982. Distribution and kinetics of membrane dielectric polarization. I. Long-term inactivation of gating currents. *Journal of General Physiology.* 79:21–40.

Bechem, M., and L. Pott. 1985. Removal of Ca²⁺ current inactivation in dialysed guinea-pig atrial cardioballs by Ca²⁺ chelators. *Pflugers Archiv.* 404:10–20.

Brum, G., and E. Ríos. 1987. Intramembrane charge movement in frog skeletal muscle fibers. Properties of charge 2. *Journal of Physiology.* 387:489–517.

Byerly, L., and J. W. Moody. 1984. Intracellular calcium ions and calcium current in perfused neurones of the snail *Limnea Stagnalis. Journal of Physiology.* 352:637–652.

Campbell, D. L., W. R. Giles, K. Robinson, and E. F. Shibata. 1988. Studies of the sodium-calcium exchanger in bull-frog atrial myocytes. *Journal of Physiology.* 403:317–340.

Catterall, W. A. 1988. Structure and function of voltage-sensitive channels. *Science.* 242:50–61.

Cavalie, A., R. Ochi, D. Pelzer, and W. Trautwein. 1983. Elementary currents through Ca²⁺ channels in Guinea pig myocytes. *Pflugers Archiv.* 398:284–297.

Chad, J. E., and R. Eckert. 1984. Calcium domains associated with individual channels can account for anomalous voltage relations of Ca-dependent responses. *Biophysical Journal.* 45:993–999.

Droogmans, G., and B. Nilius. 1989. Kinetic properties of the cardiac T-type calcium channels in the guinea pig. *Journal of Physiology.* 419:627–650.

Dupont, J. L., J. L. Bossu, and A. Feltz. 1986. Effect of internal calcium concentration on calcium currents in rat sensory neurones. *Pflugers Archiv.* 406:433–435.

Eckert, R., and J. E. Chad. 1984. Inactivation of Ca²⁺ channels. *Progress in Biophysics and Molecular Biology.* 1948:215–267.

Field, A. C., C. Hill, and G. D. Lamb. 1988. Asymmetric charge movement and calcium currents in ventricular myocytes of neonatal rat. *Journal of Physiology.* 406:277–297.

Guy, H. R., and P. Seetharamulu. 1986. Molecular model of the action potential sodium channel. *Proceedings of the National Academy of Sciences, USA.* 83:508–512.

Hadley, R. W., and W. J. Lederer. 1989. Intramembrane charge movement in guinea pig and rat ventricular myocytes. *Journal of Physiology.* 415:601–624.

Hadley, R. W., and W. J. Lederer. 1991. Ca^{2+} and voltage inactivate Ca^{2+} channels in guinea pig ventricular myocytes through independent mechanisms. *Journal of Physiology.* 444:257–268.

Hodgkin, A. L., and B. Katz. 1949. The effect of sodium ions on the electrical activity of the giant axon of the squid. *Journal of Physiology.* 108:37–77.

Johnson, B. D., and L. Byerly. 1993. Photo-released intracellular Ca^{2+} rapidly blocks Ba^{2+} current in *Lymnaea* neurones. *Journal of Physiology.* 462:321–347.

Kohlhardt, M., H. Krause, M. Kubler, and A. Herdey. 1975. Kinetics of inactivation and recovery of the slow inward current in the mammalian ventricular myocardium. *Pflugers Archiv.* 355:1–17.

Kostyuk, P. G. 1984. Intracellular perfusion of nerve cells and its effects on membrane currents. *Physiological Reviews.* 64:435–453.

Neely, A., X. Wei, L. Birnbaumer, and E. Stefani. 1993. Calcium-dependent inactivation of cardiac calcium channel $\alpha 1 \beta 2$ subunits and a deletion mutant of $\alpha 1$ expressed in *Xenopus* oocytes. *Biophysical Journal.* 64:202a. (Abstr.)

Neher, E. 1986. Concentration profiles of intracellular calcium in the presence of a diffusible chelator. *Experimental Brain Research.* 14:80–96.

Ohya, Y., K. Kitamura, and H. Kuriyama. 1988. Regulation of calcium current by intracellular calcium in smooth muscle cells of rabbit portal vein. *Circulation Research.* 62:375–383.

Pizarro, G., R. Fitts, I. Uribe, and E. Ríos. 1989. The voltage sensor of exitation-contraction coupling in skeletal muscle. Ion dependence and selectivity. *Journal of General Physiology.* 94:405–428.

Press, W. H., B. P. Flannery, S. A. Teukolsky, and W. T. Vetteriling. 1988. Numerical recipes in C. *In* The Art of Scientific Computing. Cambridge University Press, NY. 566–580.

Reuter, H. 1967. The dependence of slow inward current in Purkinje fibres on the extracellular calcium concentration. *Journal of Physiology.* 192:479–492.

Rose, W. C., C. W. Balke, W. G. Wier, and E. Marban. 1992. Macroscopic and unitary properties of physiological ion flux through L-type Ca^{2+} channels in guinea-pig heart cells. *Journal of Physiology.* 456:267–284.

Rosenberg, R. L., and J. A Haack. 1993. Permeation of calcium ions through reconstituted L-type calcium channels increases inactivation rates. *Biophysical Journal.* 64:5a. (Abstr.)

Shirokov, R., R. Levis, and E. Ríos. 1993. A simple model of V- and Ca^{2+}-dependent inactivation of L-type Ca^{2+} channels. 1993. *Biophysical Journal.* 64:202a. (Abstr.)

Shirokov, R., R. Levis, N. Shirokova, and E. Ríos. 1992. Two classes of gating charge from L-type Ca^{2+} channels in guinea pig ventricular myocytes. *Journal of General Physiology.* 99:863–895.

Shirokov, R., R. Levis, N. Shirokova, and E. Ríos. 1993. Charge in L-type Ca^{2+} channels is converted by voltage- but not Ca^{2+}-dependent inactivation. *Biophysical Journal.* 64:116a. (Abstr.)

Simon, B. J., and K. G. Beam. 1985. The influence of transverse tubular delays on the kinetics of charge movement in mammalian skeletal muscle. *Journal of General Physiology.* 85:21–42.

Stern, M. D. 1992. Buffering of calcium in the vicinity of a channel pore. *Cell Calcium.* 13:183–192.

Stuhmer, W., F. Conti, M. Stocker, O. Pongs, and S. H. Heinemann. 1991. Gating currents of inactivating and non-inactivating potassium channels expressed in *Xenopus* oocytes. *Pflugers Archiv.* 418:423–429.

Tsien, R. W., P. Hess, E. W. McCleskey, and R. L. Rosenberg. 1987. Calcium channels: mechanisms of selectivity, permeation, and block. *Annual Review of Biophysics Biophysical Chemistry.* 16:265–290.

Yue, D. T., P. H. Backx, and J. P. Imredy. 1990. Calcium-sensitive inactivation in the gating of single calcium channels. *Science.* 250:1735–1738.